Published in final edited form as:
Structure. 2011 August 10; 19(8): 1170–1181. doi:10.1016/j.str.2011.05.010.

Structural basis of the anti-HIV activity of the cyanobacterial *Oscillatoria Agardhii* agglutinin

Leonardus M.I. Koharudin and **Angela M. Gronenborn***
Department of Structural Biology, School of Medicine, University of Pittsburgh, Biomedical Science Tower 3, 3501 Fifth Avenue, Pittsburgh, PA 15260, USA

Summary

The cyanobacterial *Oscillatory Agardhii* agglutinin (OAA) is a recently discovered HIV-inactivating lectin that interacts with high-mannose sugars. NMR binding studies between OAA and α3,α6-mannopentaose (Manα(1-3)[Manα(1-3)[Manα(1-6)]Manα(1-6)]Man), the branched core unit of Man-9, revealed two binding sites at opposite ends of the protein, exhibiting essentially identical affinities. Atomic details of the specific protein-sugar contacts in the recognition loops of OAA were delineated in the high-resolution crystal structures of free and glycan-complexed protein. No major changes in the overall protein structure are induced by carbohydrate binding, with essentially identical apo- and sugar-bound conformations in binding site 1. A single peptide bond flip at W77-G78 is seen in binding site 2. Our combined NMR and crystallographic results provide structural insights into the mechanism by which OAA specifically recognizes the branched Man-9 core, distinctly different from the recognition of the D1 and D3 arms at the non-reducing end of high-mannose carbohydrates by other antiviral lectins.

Introduction

The human immunodeficiency virus (HIV) displays on its surface the envelope glycoprotein gp120 that is pivotal for viral attachment to the host cell (Eckert and Kim, 2001; Freed and Martin, 1995). Gp120 is remarkably rich in high mannose N-linked sugars (Doores et al., 2010; Kwong et al., 1998), contributing ~50% of the molecular weight of gp120 (Ji et al., 2006). Over the last decade, various lectins were discovered that exerted anti-HIV activity by specifically and tightly binding to gp120-attached glycans (Bokesch et al., 2003; Boyd et al., 1997; Chiba et al., 2004; Mori et al., 2005; Pohlmann et al., 2001; Yamaguchi et al., 1999), spurring continous searches for other HIV-inactivating members of the lectin family.

One such protein was discovered in the cyanobacterium *Oscillatory Agardhii* (named *Oscillatory Agardhii* Agglutinin; OAA). It also exhibits potent anti-HIV activity, mediated by high affinity binding to the high mannose glycans on gp120 (Sato et al., 2007). We recently determined the three-dimensional structure of OAA by X-ray crystallography, revealing a novel, compact, β-barrel-like architecture (Koharudin et al., 2010).

*Correspondence: Angela M. Gronenborn : amg100@pitt.edu, Phone: (412) 648 9959, Fax: (412) 648 9008.

The authors declare no conflict of interest.

In order to elucidate the atomic basis of OAA's activity, we have now determined the structure of an OAA-carbohydrate complex. Our initial efforts aimed at crystallizing the OAA/Man-9 complex, either through soaking or co-crystallization, were unsuccessful. The reason for our failure can be attributed to the presence of N-cyclohexyl-3-aminopropane-sulfonic acid (CAPS) in the crystallization buffer: the crystals contained protein with two bound CAPS molecules in the structure, located in the carbohydrate binding sites that were delineated by NMR titration on the surface of OAA (Koharudin et al., 2010), at opposite ends of the protein. Site 1 is formed by β-strands from the N- and C-terminal ends of the polypeptide and exhibited somewhat lower affinity than site 2 that comprises residues in the middle of the protein sequence.

The minimal substructure of Man-9 that exhibited high affinity and specific binding to OAA is α3,α6-mannopentaose (or Manα(1-3)[Manα(1-3)[Manα(1-6)]Manα(1-6)]Man pentasaccharide), the branched core unit of Man-9 (Sato et al., 2007). Given that α3,α6-mannopentaose is readily and commercially available, in contrast to Man-9, we focused our co-crystallization efforts on α3,α6-mannopentaose.

Here, we report the crystal structure of OAA, complexed with α3,α6-mannopentaose and an additional apo-structure that is devoid of any small organic molecules in the sugar binding sites. Using NMR spectroscopy, we identified which residues in each binding site are influenced by α3,α6-mannopentaose binding in solution and determined their binding affinities. A detailed comparison between the free and bound protein conformation revealed that no significant conformational changes are induced by sugar binding, except in binding site 2. In particular, we note a flip in the orientation of the peptide bond between W77 and G78.

All together, our combined NMR spectroscopic and X-ray crystallographic results provide the first atomic details of OAA's interaction with the core epitope of Man-9 and aid in our understanding the protein's potent anti-HIV activity. In addition, our structural data adds important novel information to the growing body of knowledge about antiviral lectins that, in turn, may be exploited for glycan targeting on gp120 in the fight against HIV transmission.

Results and Discussion

OAA strongly and specifically binds to α3,α6-mannopentaose in solution

We previously showed by NMR spectroscopy that OAA binds to Man-9 in solution (Koharudin et al., 2010). Here, in order to delineate the atomic details of the binding interface, we investigated the interaction with α3,α6-mannopentaose, the minimal unit of Man-9 recognized by OAA (Sato et al., 2007).

Binding between OAA and α3,α6-mannopentaose is in slow exchange on the NMR chemical shift scale, suggesting a relatively tight interaction. Backbone resonance assignments for the sugar-bound protein were obtained using 3D HNCACB and HN(CO)CACB spectra recorded for an OAA sample in the presence of excess of α3,α6-mannopentaose. The 2D ^{1}H-^{15}N HSQC spectra of the apo- and α3,α6-mannopentaose-bound OAA, annotated with the amide backbone assignments, are provided in Figures 1A and 1B, respectively. Similar to the apo spectrum, the sugar-bound spectrum exhibits well-dispersed and narrow resonances. All expected amide cross-peaks were observed, except for residue N69, whose amide resonance is broadened beyond detection in both spectra.

Binding isotherms for the interaction between α3,α6-mannopentaose and OAA were derived from signal intensities of selected amide resonances in the 2D ^{1}H-^{15}N HSQC spectra at

seven OAA (40 μM) to α3,α6-mannopentaose molar ratios: 1:0 (free protein), 1:0.25, 1:0.5, 1:1, 1:1.5, 1:2, and 1:3. At the 1:3 ratio, the protein is completely saturated with the carbohydrate. Superpositions of these spectra are provided in Figures 2A to 2F with the free protein spectrum always shown in black (Figures 2A to 2F) and spectra at 1:0.25, 1:0.5, 1:1, 1:1.5, 1:2 and 1:3 molar ratios in red (Figure 2A), green (Figure 2B), blue (Figure 2C), yellow (Figure 2D), magenta (Figure 2E), and cyan (Figures 2F and S1), respectively. Note that the 1:3 molar ratio translates to 1.5 sugar molecules per protein binding site. Residues whose amide chemical shifts are significantly changed upon sugar binding are labeled by residue name and number, with those in binding sites 1 and 2 labeled in black and red, respectively. The free and bound resonances for the same residue are connected by dashed lines. Already at the molar ratio of 1:0.25 (inset in Figure 2A), a very small effect on R28 can be observed. However, at the molar ratio of 1:1, where each binding site would be half saturated for identical sugar affinities, the bound resonances of G60 and G127 (equivalent residues in binding sites 2 and 1) are of equal intensities (within the error of the measurements; inset in Figure 2C). Similar observations hold for other resonances as well, providing strong evidence that α3,α6-mannopentaose binds to sites 1 and 2 with very similar affinities. This is different from our findings with Man-9 where we noted a somewhat higher affinity for binding in site 2.

All chemical shift differences between free OAA and sugar-bound resonances, determined at saturation, are displayed along the polypeptide chain in Figure 2G. As can be appreciated, the most strongly affected residues are located in the loop regions, connecting strands β1-β2 and β9-β10 (site 1 – black bars) and connecting strands β4-β5 and β6-β7 (site 2 – red bars), respectively. Smaller changes are present for the loops connecting β7-β8 (site 1 black bars) and β2-β3 (site 2 red bars) Resonances with chemical shift differences of > 0.1 ppm (> 1 standard deviation of ~0.095) include residues L3, E7-S13, A15, W17-W23, E95, L114, T117, M118, Y120, E123-F128 in binding site 1 and residues I25, S27, R28, V34, M51-A54, E56-F61, A63, E72, Q76-D80, A82, W84, S86, G88, and L92 in binding site 2. A simple qualitative comparison reveals a very close resemblance in patterns for perturbations around β4-β5 and β9-β10, while for the β1-β2 and β6-β7 regions some variability is observed, with W10 exhibiting the largest sugar-induced shift of all resonances. The set of perturbed resonances is very similar to those detected previously with Man-9, indicating that α3,α6-mannopentaose provides essentially all the determinants necessary for the interaction.

Determination of apo and α3,α6-mannopentaose-bound OAA structures

Having established that OAA strongly and specifically binds to α3,α6-mannopentaose, we aimed to obtain crystals of the OAA-α3,α6-mannopentaose complex, either by co-crystallization or soaking. Since our previously determined apo crystal structure contained bound CAPS molecules in the carbohydrate binding sites on OAA that prevented glycan binding in the crystal, we removed CAPS from the crystallization mix and varied precipitant composition. Crystals of both apo and α3,α6-mannopentaose-bound OAA were obtained using 2.0 M $(NH_4)2SO_4$ and 0.1 M Tris.HCl (pH 8.5). The protein crystallized in space group $P2_12_12_1$, with one protein molecule per asymmetric unit, different from the previously determined structure of CAPS-bound OAA in space group P_1. The current apo-OAA structure was solved by molecular replacement using the previously determined structure of OAA (PDB:3OBL), comprising residues 2 to 133 as the structural probe in PHASER (McCoy, 2007). The final model was refined to 1.55 Å resolution with R=18.2% and R_{free}= of 19.6%. No bound organic molecules were present. We also obtained crystals of α3,α6-mannopentaose-bound OAA, using the same crystallization condition and solutions of OAA-carbohydrate at protein:carbohydrate ratios of 1:2, 1:3, or 1:4 and a protein concentration of 40 mg/ml. All mixtures yielded well diffracting crystals and we solved the complex structure using a crystal that was obtained with the 1:3 protein:carbohydrate ratio.

The OAA-α3,α6-mannopentaose complex crystallized in space group of $P2_12_12_1$ with one protein molecule per asymmetric unit. The crystallographic phase was solved by molecular replacement using the new apo OAA structure as the structural probe in PHASER (McCoy, 2007) and the final model was refined to 1.65 Å resolution with R=18.9% and R_{free}= of 22.8%.

Overall comparison of apo and α3,α6-mannopentaose-bound OAA structures

The structures of the apo- and α3,α6-mannopentaose-bound OAA are very similar, with the compact ten-stranded anti-parallel β-sheet barrel essentially identical (Figures 3A and 3B). The first five β-strands (colored in white and light green for the apo and the complex structures, respectively) comprise residues 2 to 66 from the first amino acid sequence repeat. The next five β-strands (colored in purple and light blue for the apo and the complex structures, respectively) are composed of residues 70 to 133 from the second sequence repeat. A short linker (colored in orange in each structure), comprising residues G67 to N69, connects these two-sequence repeats. The additional electron density at opposite ends of the protein molecule permitted the placement of a α3,α6-mannopentaose molecule into each site, and in the final density, an excellent fit of the atomic structure of two bound α3,α6-mannopentaose molecules, one per carbohydrate binding site of OAA, is observed (Figures 3C and 3D).

Although the free and the α3,α6-mannopentaose-bound OAA structure are very similar, exhibiting root mean square deviations (r.m.s.d) for backbone and heavy atoms (residues A2 to T133) of 0.51 and 0.81 Å, respectively (Figure 3E), a few conformational differences, especially in the loops connecting strands β2-β3, β4-β5, and β6-β7 (Figure 3E) can be discerned. These loops are part of the carbohydrate binding site 2 in OAA (Figure S2). Additional very small variations are also observed in the short linker region comprising residues G67 to N69 (Figure 3E), most likely indicating conformational flexibility, since the N69 amide resonance in solution is broadened in the ^{1}H-^{15}N HSQC by exchange on the millisecond time scale. Very small differences are also observed in the loop region connecting strands β1-β2 (Figure S2) that lines the carbohydrate binding site 1 (Figures 2G and S2). Therefore, within the error of the coordinates, essentially no significant difference in the conformation of binding site 1 in the free and carbohydrate-bound state of OAA is discernible. For binding site 2, on the other hand, a small, but clear local conformational difference is observed between the free- and sugar-bound protein.

Structural basis for carbohydrate binding and specificity

The structure of the OAA-α3,α6-mannopentaose complex (Figure 3) permits an assessment of the specific contacts between the carbohydrate and OAA at the atomic level. α3,α6-mannopentaose represents the core structure of Man-9 (Figure 4A) and the sugar binding pockets of site 1 and site 2 on OAA are very similar (Figures 4B and 4C). OAA's carbohydrate recognition sites comprise short clefts, residing between the loops on the surface of the protein. They are formed primarily by residues in the loops connecting strands β1-β2 and β9-β10 and those connecting strands β4-β5 and β6-β7 for sites 1 and 2, respectively. These two loops are in direct contact with the carbohydrate, particularly residues W10-G12 and E123-G124, located in the loop that connects strands β1-β2 and strands β9-β10 in binding site 1, and residues E56-G57 and W77-G79 in the loop, connecting strands β4-β5 and β6-β7 in binding site 2. The loops connecting strands β7-β8 in site 1 or strands β2-β3 in site 2 are slightly more remote, and contain amino acids with long side chains that directly interact with the carbohydrate, such as R95 in site 1 or R28 in site 2.

The M4'α(1-6)M3 disaccharide unit of the α3,α6-mannopentaose is in closest contact with the protein (Figures 4B and 4C), and of the five-mannose carbohydrate moieties, the

M4α(1-3)M3 disaccharide is located deep inside the binding pocket while the M5'α(1-3)[M5"α(1-6)]M4' trisaccharide unit is pointing outwards. Overall, the branch point sits in the center of the binding site and all mannose units are splayed out from the center. For the M4α(1-3)M3 unit, the pyranose ring of M3 is stacked on top of the indole ring of the W10 and W77 side chains in site 1 and site 2, respectively. The pyranose ring of M4 is flanked by the long side chains of residues R95 and R28 in site 1 and 2, respectively. On the other side of the cleft, where the M5'α(1-3)[M5"α(1-6)]M4' trisaccharide is located, the pyranose ring of M5' is flanked by residues in the loop connecting strands β1-β2 and β6-β7 in site 1 and 2, respectively, while the pyranose rings of M5'' and M4' are flanked by residues in the β9-β10 and β4-β5 loops for site 1 and 2, respectively.

Of all the contacts in the binding sites it appears that the hydrophobic interaction between the aromatic side chain of W10 in site 1 and W77 in site 2 with the pyranose ring of M3 plays a critical role. In addition, several polar interactions are also observed. In particular, hydrogen bonds between the hydroxyl groups of the carbohydrate and main chain amide groups are present, augmented by several contacts with side chains. In binding site 1 (Figure 4D), hydrogen bonds are formed between the backbone amide of G11 and the C5 hydroxyl group of M5' (2.86 Å), the backbone amide of G12 and the C6 hydroxyl group of M5' (2.87 Å), the backbone amide of G124 and the C5 hydroxyl group of M4' (3.00 Å), and the backbone amide of G124 and the C6 hydroxyl group of M4' (3.15 Å). Side chain interactions in binding site 1 include hydrogen bonds between the C4 hydroxyl group of M3 and the side chain carboxyl group of E123 (2.81 Å) and between the C4 hydroxyl group of M3 and the terminal guanidinium group of R95 (2.89 Å). Equivalent hydrogen bonds are found in binding site 2 (Figure 4E). Hydrogen bonds between the backbone amide of G78 and the C5 hydroxyl group of M5' (2.93 Å), the backbone amide of G79 and the C6 hydroxyl group of M5' (2.83 Å), the backbone amide of G57 and the C5 hydroxyl group of M4' (2.92 Å), and the backbone amide of G57 and the C6 hydroxyl group of M4' (3.20 Å) are present. Side chain hydrogen bonding is observed between the C4 hydroxyl group of M3 and the side chain carboxyl group of E56 (2.73 Å) and between the C4 hydroxyl group of M3 and the terminal guanidinium group of R28 (2.84 Å).

Comparison of the carbohydrate binding sites within the apo- and α3,α6-mannopentaose-bound structures

The extremely similar interactions between the sugar and the protein in the binding sites are accompanied by highly homologous conformations of the polypeptide chains in these regions (Figure S3A). Only a small variation in the orientations of the W10 and W77 side chains can be discerned and the pyranose rings of the M3, M4, and M5" units in the two carbohydrates are almost identical. A best-fit superposition for the two binding regions (residues S94 - L132 and L3 - W23 for site 1 and residues S27 – L65 and S70 – W90 for site 2, respectively) yields a backbone r.m.s.d. value of 0.38 Å. The small difference in the M5" conformation at the solvent-exposed end of the carbohydrate chains is most likely a reflection of the inherent flexibility of the sugar when not held in place by the protein. Indeed, M3, M4', and M5' are completely indistinguishable in the two sites and only very minor differences are seen for M4 and M5" (Figure S3B).

Surprisingly, however, comparison of the two carbohydrate binding sites in the apo-structure revealed some differences (Figure S3C). In the free protein, the orientation of the peptide bond between W10 and G11 (binding site 1) and W77 and G78 (binding site 2) is flipped, with the carbonyl oxygens of W10 and W77 pointing in opposite directions. Upon sugar binding, the conformation in binding site 1 is essentially unaltered (Figure 5A), whereas α3,α6-mannopentaose binding to site 2 changes the orientation of the W77/ G78 peptide plane to that present in the free and bound state of site 1 (Figure 5B). This type of conformational change seen for free versus bound states in proteins has frequently been

discussed in terms of the general, mechanistic question of conformational selection versus induced fit (Hammes et al., 2009; Wlodarski and Zagrovic, 2009). We therefore carefully assessed whether the conformations in the free protein are truly representing a ligand-free unoccupied binding site.

To that end, we evaluated whether crystal packing could affect the conformation of the two binding sites in the apo structure. Indeed, a clear difference was found for the two sites: the loop region connecting strands β1 and β2, comprising residues G11-P16, is surrounded by several neighboring symmetrically related protein molecules, with one neighboring molecule forming hydrogen bonds with two loop residues (Figure 6A). In particular, the carbonyl oxygen of G11 in the loop accepts a H-bond from the side chain amide of N69 and the amide proton of S13 donates a hydrogen bond to the side chain carboxyl of E96. No such interactions are present around the corresponding loop in binding site 2 (Figure 6B), suggesting that the conformation in binding site 1 in the apo-crystal structure is induced by protein-protein contacts in the crystal lattice.

In order to further confirm that the behavior of the loops in binding sites 1 and 2 in solution is basically identical, we recorded NMR relaxation experiments for the apo protein (Figures 6C–6E). Comparison of the T_1, T_2, and heteronuclear NOE data for the two pertinent loops (β1-β2; β6-β7) reveals essentially the same values for the equivalent residues. In addition, we explored different temperatures for data collection, both for the crystal as well as for the NMR, since differences between NMR and X-ray results could have been caused by 'freezing out' conformations at cryogenic temperatures in the crystal. X-ray data collected at room temperature (Figure S4) and the 2D ^{1}H-^{15}N HSQC spectrum at 277.4 K (Figure S5), however, did not suggested that in the cryogenic X-ray structure the bound conformation was fortuitously selected. We therefore conclude that both loop regions in the free protein are flexible and that crystal packing effects around the carbohydrate binding site 1 forces the conformation of the β1-β2 loop into the conformation observed in the carbohydrate-bound structure.

Comparison with other mannose-binding lectins

Our present structure also permits a detailed comparison between several binding modes observed in other Man-9 interacting lectins. For example, Cyanovirin-N (Boyd et al., 1997), DC-SIGN (Pohlmann et al., 2001), Scytovirin (Bokesch et al., 2003), Griffithsin (Mori et al., 2005), MVL (Yamaguchi et al., 1999), and Actinohivin (Chiba et al., 2004), all recognize different epitopes of Man-9. In particular, Cyanovirin-N specifically recognizes Manα(1-2)Man linked mannose substructures in the D1 and D3 arms of Man-9 (Barrientos et al., 2006; Bewley, 2001; Botos et al., 2002), DC-SIGN preferentially interacts with the Manα(1-3)Manα(1-6)Man trisaccharide (Feinberg et al., 2001) and MVL specifically interacts with the Manα(1-6)Manβ(1-4)GlcNAcβ(1-4)GlcNAc tetrasaccharide (Williams et al., 2005). In addition, sugar binding studies for Scytovirin and Actinohivin revealed specificities for Man⟨(1-2)Man⟨(1-6)Man⟨(1-6)Man (McFeeters et al., 2007) and Manα(1-2)Man (Tanaka et al., 2009), respectively. The structure of Griffithsin contained three single mannose units (Ziolkowska et al., 2006) and its engineered monomeric variant, complexed with Man-9 reveals that each reducing end mannose of the triantennary Man-9 interacts with each of the three available binding sites (Moulaei et al., 2010).

Most of the above lectins recognize the reducing or non-reducing end mannoses of Man-9, whereas OAA recognizes the core structure of the triantennary Man-9. In that regard it was interesting to note, that the mode of OAA's carbohydrate recognition resembled that of OS-9, a lectin involved in ER-associated degradation (ERAD) (Satoh et al., 2010). A detailed comparison of the interactions around the central beta mannose unit (BMA) for the two complexes is provided in Figure 7. In both carbohydrate-bound structures, the BMA

unit is flanked by a Trp residue side chain (W10 or W77 in OAA and W117 in OS-9). The importance of this Trp residue as a critical contact was confirmed for OAA by mutagenesis: mutation of W77 to A77 completely abolished carbohydrate binding to site 2 (Figure S6). In the OS-9 structure, a second Trp side chain appears to also contribute to sugar binding: the W118 side chain Nε1H forms a hydrogen with the C5 hydroxyl group of M4'. No such residue is present in OAA. However, in the α3,α6-mannopentaose-bound OAA structure, the C5 hydroxyl group of M4' is also involved in a hydrogen bond, namely with the amide group of G124 in site 1 or the amide group of G57 in site 2. There is a distinct difference, on the other hand, in the completeness of the bound sugar moiety. Only three mannose units of the α3,α6-mannopentaose glycan could be modeled in the structure of OS-9 complex, whereas all five mannose units are clearly seen in the OAA complex, all placed within well defined electron density (Figure 3C).

Conclusion

We have determined the crystal structures of apo and α3,α6-mannopentaose-bound OAA at a resolution of 1.55 Å and 1.65 Å, respectively. In addition, we also solved the crystal structure of apo OAA at room temperature at 1.60 Å. Comparison between the apo and glycan-bound structures revealed no major conformational changes in the overall polypeptide backbone of the protein upon sugar binding, except for a flip in the peptide bond between W77 and G78 in the carbohydrate binding site 2. Interestingly, our α3,α6-mannopentaose-bound OAA crystal structure supports one of the two models that we proposed in our earlier work (Koharudin et al., 2010), in which the chitobiose unit is pointing upwards and is exposed to the solvent, with the D1 arm pointing in the direction of strand β2. While the complex crystal structure supports our previous NMR titration experiments that also indicated no interactions between OAA and the chitobiose unit, this finding is at variance with previous data reported by Sato et al. (2007). We believe that the discrepancy with respect to the involvement of the chitobiose unit most likely originates from the different methodologies employed and may be caused by the reduced (ring-opened) state of the M3 in the pyridylaminated pentamannose derivative used in Sato et al. (2007).

Comparison between the present apo- and carbohydrate-bound structures and the previously determined CAPS containing OAA structure (Koharudin et al., 2010) revealed that the CAPS- and α3,α6-mannopentaose-bound structures are more similar than the CAPS-bound and free ones. In particular, the regions of two binding sites are almost identical (Figure S7). This implies that CAPS binding in the previous apo structure mimics the effect seen in the genuine 'carbohydrate-bound' structure.

The carbohydrate recognition of OAA of Man-9 is unique in comparison to other anti-viral lectins. While most of the known HIV-inactivating lectins recognize the reducing or non-reducing end mannoses of Man-9, OAA recognizes the core structure of the triantennary Man-9. Therefore, it may be possible to explore whether any synergistic action between core and terminal mannose-recognizing lectins can be harnessed for targeting gp120 in the fight against HIV transmission.

Experimental procedures

Protein expression, purification, and crystallization

The protein was expressed and purified as described previously (Koharudin et al., 2010). Briefly, the synthetic OAA gene encoding residues 1 133 (Sato and Hori, 2009) was cloned into the pET-26b(+) expression vector (Novagen), using NdeI and XhoI restriction sites at the 5' and 3' ends, respectively. *E. coli* Rosetta2 (DE3) cells (Novagen) were transformed

with the pET-26b(+)-OAA vector for protein expression. Cells were initially grown at 37°C, induced with 1 mM IPTG at 16°C, and grown for ~18 h at 16°C for protein expression.

Protein was prepared from the soluble fraction of *E. coli* after opening the cells by sonication. The cell lysate was centrifuged to remove cell debris and, after centrifugation, the supernantant was dialyzed over night against 20 mM Tris-HCl buffer (pH 8.5). Further purification involved anion-exchange chromatography on a Q(HP) column (GE Healthcare), using a linear gradient of NaCl (20-1000 mM) for elution, followed by gel filtration on Superdex75 (GE Healthcare) in 20 mM Tris-HCl buffer, 100 mM NaCl, 3 mM NaN_3, (pH 8.0). Purified protein fractions were collected and concentrated up to 40 mg/ml using centriprep devices (Millipore).

For crystallization of the apo and α3,α6-mannopentaose-bound OAA, we modified the crystallization conditions used to obtain the previous apo structure of OAA in the presence of bound CAPS molecules (1.2 M NaH_2PO_4/0.8 M K_2HPO_4 (pH 5.5), 0.2 M Li_2SO_4, 0.1 M CAPS (pH 10.5) or 2.0 M $(NH_4)2SO_4$ (pH 5.4), 0.2 M Li_2SO_4, 0.1 M CAPS (pH 10.5)). The CAPS buffer was replaced with Tris-HCl (pH 8.5, 8.0, and 7.5), HEPES (pH 7.0), NaPhosphate (pH 6.0), and NaAcetate (pH 5.0). The precipitants (either NaH_2PO_4/K_2HPO_4 (pH 5.5) or $(NH_4)2SO_4$ (pH 5.4)) were kept, but their concentrations were varied from 1.6 to 2.4 M for NaH_2PO_4/K_2HPO_4 and from 1.6 to 2.8 M for $(NH_4)2SO_4$. Similarly, the salt (Li_2SO_4) concentration was also varied from 0 to 0.25 M. All crystallization trials were carried out by the sitting drop vapor diffusion method at room temperature using drops consisting of 2 μl protein and 2 μl of reservoir solutions at a protein concentration of 40 mg/ml. Well diffracting crystals for both the apo- and carbohydrate-bound protein were found with 2.0 M $(NH_4)2SO_4$ and 0.1 M Tris-HCl (pH 8.5). The crystals for the carbohydrate-bound protein were obtained by co-crystallization using a mixture of protein and α3,α6-mannopentaose at molar ratios of 1:2, 1:3, or 1:4, with the protein concentration kept at 40 mg/ml, using the same volume ratio and conditions as for apo protein crystallization.

Diffraction data collection and structure determination of apo and OAA

X-ray diffraction data for both apo- and glycan-bound crystals were collected up to 1.50 and 1.65 Å resolution, respectively, on flash-cooled crystals (-180°C) using a Rigaku FR-E generator with a R-AXIS IV image plate detector at a wavelength corresponding to the copper edge (1.54 Å). All diffraction data were processed, integrated, and scaled using d*TREK software (Pflugrath, 1999), and eventually converted to mtz format using the CCP4 package (Collaborative computational project, 1994). All pertinent statistics are summarized in Table 1. The unit-cell dimensions of the $P2_12_12_1$ apo crystal were a = 38.90 Å, b = 40.09 Å, and c = 69.00 Å (α, β, and γ = 90°) and for the $P2_12_12_1$ α3,α6-mannopentaose-bound crystal a = 35.19 Å, b = 49.07 Å, and c = 69.25 Å (α, β, and γ = 90°), with an estimated solvent content of ~37% (V_m = 1.94 $Å^3$/Da) and 43% (V_m = 2.15 $Å^3$/Da), respectively, based on Matthews Probability Calculator (http://www.ruppweb.org/Mattprob/). Both crystals contain one polypeptide molecule per asymmetric unit.

Phases were determined by molecular replacement using the previously determined structure of OAA (PDB:3OBL) (Koharudin et al., 2010) as structural probe in PHASER (McCoy, 2007). After generation of the initial model, the chain was re-built using the program Coot (Emsley and Cowtan, 2004). Iterative refinement was carried out by alternating between manual re-building in Coot (Emsley and Cowtan, 2004) and automated refinement in REFMAC (Murshudov et al., 1997). Similar procedures were adopted for the diffraction data collected from the complex crystal. In the later case, the structure obtained from the new apo protein was used as the structural probe for molecular replacement.

All final models exhibit clear electron density for all residues (2-133), as expected. In the complex, additional electron density was present in the asymmetric unit in the region of the two carbohydrate binding sites of OAA. The final apo structure was well defined with an R-factor of 18.2% and a free R of 19.6%. 97.7% and 100% of all residues are located in the favored and allowed regions of the Ramachandran plot, respectively, and no residues in the disallowed region as evaluated by MOLPROBITY (Davis et al., 2007). The extra density in both sites permitted fitting of a α3,α6-mannopentaose molecule into each binding site. The final complex structure is well refined with an R-factor of 18.9% and a free R of 22.8%. 97.8%, and 100% of all residues lie in the favored and allowed regions of the Ramachandran plot, respectively. A summary of the data collection parameters as well as pertinent structural statistics for both structures is provided in Table 1. All structural figures were generated with Chimera (Pettersen et al., 2004) or PyMOL (DeLano, 2002). The atomic coordinates and diffraction data for apo and the α3,α6-mannopentaose-bound structures have been deposited in the RCSB Protein Data Bank under accession codes 3S5V and 3S5X for the apo and complex forms, respectively.

Room temperature diffraction data collection and structure determination of apo OAA

X-ray diffraction data for the apo protein crystal at room temperature were collected at 25°C up to 1.60 Å resolution, using a Rigaku FR-E generator with Saturn 944 CCD detector at a wavelength corresponding to the copper edge (1.54 Å). Diffraction data were processed, integrated, and scaled using d*TREK software (Pflugrath, 1999), and eventually converted to mtz format using the CCP4 package (Collaborative computational project, 1994). All pertinent statistics are summarized in Table 1. The unit-cell dimensions of the $P2_12_12_1$ apo crystal were a = 39.47 Å, b = 40.66 Å, and c = 70.37 Å (α, β, and γ = 90°). The crystal contains one polypeptide molecule per asymmetric unit. Phases were determined by molecular replacement using the structure of apo OAA determined at cryogenic temperature, comprising residues 2 to 133 as the structural probe. The final model exhibits clear electron density for all residues (2-133). The room temperature apo structure was refined to 1.60 Å resolution, with an R-factor of 18.1% and a free R of 23.0%. 98.5% and 100% of all residues lie in the favored and allowed regions of the Ramachandran plot, respectively, and no residues occupy the disallowed region as evaluated by MOLPROBITY (Davis et al., 2007). The atomic coordinates and diffraction data for the room temperature apo structure has been deposited in the RCSB Protein Data Bank under an accession code 3S60.

Carbohydrate binding studies by NMR Spectroscopy

3D NMR HNCACB and CBCA(CO)NH experiments (Bax and Grzesiek, 1993) were recorded for complete backbone chemical shift assignment at 26°C on a Bruker AVANCE700 spectrometer, equipped with a 5-mm triple-resonance, *z*-axis gradient cryoprobe. Spectra were recorded on a $^{13}C/^{15}N$-labeled sample in 25 mM NaAcetate, 25 mM NaCl, 3 mM NaN_3, 90/10% H_2O/D_2O (pH 5.0). The protein concentration was similar to the concentration used for crystallization at ~1.0 mM (~40 mg/mL). All spectra were processed with NMRPipe (Delaglio et al., 1995) and analyzed using NMRView (Johnson and Blevins, 1994).

Binding of α3,α6-mannopentaose (Sigma Aldrich) was investigated at 26°C using 0.040 mM ^{15}N-labeled OAA in 25 mM NaAcetate, 25 mM NaCl, 3 mM NaN_3, 90/10% H_2O/D_2O (pH 5.0) by ^1H-^{15}N HSQC spectroscopy on a Bruker AVANCE600 spectrometer. 2D ^1H-^{15}N HSQC spectra were recorded after each addition of carbohydrate with final molar ratios of protein:α3,α6-mannopentaose of 1:0, 1:0.25, 1:0.5, 1:1, 1:1.5, 1:2, and 1:3 (equivalent to 1:0, 1:0.125, 1:0.25, 1:0.5, 1:0.75, 1:1, and 1:1.5 for an individual binding site to sugar). A set of 2D ^1H-^{15}N HSQC spectra at different temperatures was recorded on a Bruker AVANCE900 spectrometer.

Supplementary Material

Refer to Web version on PubMed Central for supplementary material.

Acknowledgments

The authors thank Dr. William Furey for helpful discussions regarding the crystallographic work, Dr. Rieko Ishima for sharing her expertise in NMR relaxation, and Mike Delk for NMR technical support. This work was supported by an NIH grant to A.M.G (GM080642).

References

Barrientos LG, Matei E, Lasala F, Delgado R, Gronenborn AM. Dissecting carbohydrate-Cyanovirin-N binding by structure-guided mutagenesis: functional implications for viral entry inhibition. Protein Eng Des Sel. 2006; 19:525–535. [PubMed: 17012344]

Bax A, Grzesiek S. Methodological advances in protein NMR. Accounts of Chemical Research. 1993; 26:131–138.

Bewley CA. Solution structure of a cyanovirin-N:Man alpha 1-2Man alpha complex: structural basis for high-affinity carbohydrate-mediated binding to gp120. Structure. 2001; 9:931–940. [PubMed: 11591348]

Bokesch HR, O'Keefe BR, McKee TC, Pannell LK, Patterson GM, Gardella RS, Sowder RC 2nd, Turpin J, Watson K, Buckheit RW Jr, Boyd MR. A potent novel anti-HIV protein from the cultured cyanobacterium Scytonema varium. Biochemistry. 2003; 42:2578–2584. [PubMed: 12614152]

Botos I, O'Keefe BR, Shenoy SR, Cartner LK, Ratner DM, Seeberger PH, Boyd MR, Wlodawer A. Structures of the complexes of a potent anti-HIV protein cyanovirin-N and high mannose oligosaccharides. J Biol Chem. 2002; 277:34336–34342. [PubMed: 12110688]

Boyd MR, Gustafson KR, McMahon JB, Shoemaker RH, O'Keefe BR, Mori T, Gulakowski RJ, Wu L, Rivera MI, Laurencot CM, et al. Discovery of cyanovirin-N, a novel human immunodeficiency virus-inactivating protein that binds viral surface envelope glycoprotein gp120: potential applications to microbicide development. Antimicrob Agents Chemother. 1997; 41:1521–1530. [PubMed: 9210678]

Chiba H, Inokoshi J, Nakashima H, Omura S, Tanaka H. Actinohivin, a novel anti-human immunodeficiency virus protein from an actinomycete, inhibits viral entry to cells by binding high-mannose type sugar chains of gp120. Biochem Biophys Res Commun. 2004; 316:203–210. [PubMed: 15003531]

Collaborative computational project N. The CCP4 suite: programs for protein crystallography. Acta Crystallogr D Biol Crystallogr. 1994; 50:760–763. [PubMed: 15299374]

Davis IW, Leaver-Fay A, Chen VB, Block JN, Kapral GJ, Wang X, Murray LW, Arendall WB 3rd, Snoeyink J, Richardson JS, Richardson DC. MolProbity: all-atom contacts and structure validation for proteins and nucleic acids. Nucleic Acids Res. 2007; 35:W375–383. [PubMed: 17452350]

Delaglio F, Grzesiek S, Vuister GW, Zhu G, Pfeifer J, Bax A. Nmrpipe - a Multidimensional Spectral Processing System Based on Unix Pipes. Journal of Biomolecular NMR. 1995; 6:277–293. [PubMed: 8520220]

DeLano, WL. The PyMOL Molecular Graphics System. 2002. http://www.pymol.org

Doores KJ, Bonomelli C, Harvey DJ, Vasiljevic S, Dwek RA, Burton DR, Crispin M, Scanlan CN. Envelope glycans of immunodeficiency virions are almost entirely oligomannose antigens. Proc Natl Acad Sci U S A. 2010; 107:13800–13805. [PubMed: 20643940]

Eckert DM, Kim PS. Mechanisms of viral membrane fusion and its inhibition. Annu Rev Biochem. 2001; 70:777–810. [PubMed: 11395423]

Emsley P, Cowtan K. Coot: model-building tools for molecular graphics. Acta Crystallogr D Biol Crystallogr. 2004; 60:2126–2132. [PubMed: 15572765]

Feinberg H, Mitchell DA, Drickamer K, Weis WI. Structural basis for selective recognition of oligosaccharides by DC-SIGN and DC-SIGNR. Science. 2001; 294:2163–2166. [PubMed: 11739956]

Freed EO, Martin MA. The role of human immunodeficiency virus type 1 envelope glycoproteins in virus infection. J Biol Chem. 1995; 270:23883–23886. [PubMed: 7592573]

Hammes GG, Chang YC, Oas TG. Conformational selection or induced fit: a flux description of reaction mechanism. Proc Natl Acad Sci U S A. 2009; 106:13737–13741. [PubMed: 19666553]

Ji X, Chen Y, Faro J, Gewurz H, Bremer J, Spear GT. Interaction of human immunodeficiency virus (HIV) glycans with lectins of the human immune system. Curr Protein Pept Sci. 2006; 7:317–324. [PubMed: 16918446]

Johnson BA, Blevins RA. NMRView - a Computer-Program for the Visualization and Analysis of Nmr Data. Journal of Biomolecular NMR. 1994; 4:603–614.

Koharudin LM, Furey W, Gronenborn AM. Novel fold and carbohydrate specificity of the potent anti-hiv cyanobacterial lectin from Oscillatoria Agardhii. J Biol Chem. 2010

Kwong PD, Wyatt R, Robinson J, Sweet RW, Sodroski J, Hendrickson WA. Structure of an HIV gp120 envelope glycoprotein in complex with the CD4 receptor and a neutralizing human antibody. Nature. 1998; 393:648–659. [PubMed: 9641677]

McCoy AJ. Solving structures of protein complexes by molecular replacement with Phaser. Acta Crystallogr D Biol Crystallogr. 2007; 63:32–41. [PubMed: 17164524]

McFeeters RL, Xiong C, O'Keefe BR, Bokesch HR, McMahon JB, Ratner DM, Castelli R, Seeberger PH, Byrd RA. The novel fold of scytovirin reveals a new twist for antiviral entry inhibitors. J Mol Biol. 2007; 369:451–461. [PubMed: 17434526]

Mori T, O'Keefe BR, Sowder RC 2nd, Bringans S, Gardella R, Berg S, Cochran P, Turpin JA, Buckheit RW Jr, McMahon JB, Boyd MR. Isolation and characterization of griffithsin, a novel HIV-inactivating protein, from the red alga Griffithsia sp. J Biol Chem. 2005; 280:9345–9353. [PubMed: 15613479]

Moulaei T, Shenoy SR, Giomarelli B, Thomas C, McMahon JB, Dauter Z, O'Keefe BR, Wlodawer A. Monomerization of viral entry inhibitor griffithsin elucidates the relationship between multivalent binding to carbohydrates and anti-HIV activity. Structure. 2010; 18:1104–1115. [PubMed: 20826337]

Murshudov GN, Vagin AA, Dodson EJ. Refinement of macromolecular structures by the maximum-likelihood method. Acta Crystallogr D Biol Crystallogr. 1997; 53:240–255. [PubMed: 15299926]

Pettersen EF, Goddard TD, Huang CC, Couch GS, Greenblatt DM, Meng EC, Ferrin TE. UCSF Chimera--a visualization system for exploratory research and analysis. J Comput Chem. 2004; 25:1605–1612. [PubMed: 15264254]

Pflugrath JW. The finer things in X-ray diffraction data collection. Acta Crystallogr D Biol Crystallogr. 1999; 55:1718–1725. [PubMed: 10531521]

Pohlmann S, Baribaud F, Lee B, Leslie GJ, Sanchez MD, Hiebenthal-Millow K, Munch J, Kirchhoff F, Doms RW. DC-SIGN interactions with human immunodeficiency virus type 1 and 2 and simian immunodeficiency virus. J Virol. 2001; 75:4664–4672. [PubMed: 11312337]

Sato T, Hori K. Cloning, expression, and characterization of a novel anti-HIV lectin from the cultured cyanobacterium, *Oscillatoria agardhii*. Fish Sci. 2009; 75:743–753.

Sato Y, Okuyama S, Hori K. Primary structure and carbohydrate binding specificity of a potent anti-HIV lectin isolated from the filamentous cyanobacterium Oscillatoria agardhii. J Biol Chem. 2007; 282:11021–11029. [PubMed: 17314091]

Satoh T, Chen Y, Hu D, Hanashima S, Yamamoto K, Yamaguchi Y. Structural basis for oligosaccharide recognition of misfolded glycoproteins by OS-9 in ER-associated degradation. Mol Cell. 2010; 40:905–916. [PubMed: 21172656]

Tanaka H, Chiba H, Inokoshi J, Kuno A, Sugai T, Takahashi A, Ito Y, Tsunoda M, Suzuki K, Takenaka A, et al. Mechanism by which the lectin actinohivin blocks HIV infection of target cells. Proc Natl Acad Sci U S A. 2009; 106:15633–15638. [PubMed: 19717426]

Williams DC Jr, Lee JY, Cai M, Bewley CA, Clore GM. Crystal structures of the HIV-1 inhibitory cyanobacterial protein MVL free and bound to Man3GlcNAc2: structural basis for specificity and high-affinity binding to the core pentasaccharide from n-linked oligomannoside. J Biol Chem. 2005; 280:29269–29276. [PubMed: 15937331]

Wlodarski T, Zagrovic B. Conformational selection and induced fit mechanism underlie specificity in noncovalent interactions with ubiquitin. Proc Natl Acad Sci U S A. 2009; 106:19346–19351. [PubMed: 19887638]

Yamaguchi M, Ogawa T, Muramoto K, Kamio Y, Jimbo M, Kamiya H. Isolation and characterization of a mannan-binding lectin from the freshwater cyanobacterium (blue-green algae) Microcystis viridis. Biochem Biophys Res Commun. 1999; 265:703–708. [PubMed: 10600484]

Ziolkowska NE, O'Keefe BR, Mori T, Zhu C, Giomarelli B, Vojdani F, Palmer KE, McMahon JB, Wlodawer A. Domain-swapped structure of the potent antiviral protein griffithsin and its mode of carbohydrate binding. Structure. 2006; 14:1127–1135. [PubMed: 16843894]

Highlight

1. α3,α6-mannopentaose binds to OAA tightly and specifically at two binding sites
2. High resolution structures of free and α3,α6-mannopentaose-bound OAA are presented
3. OAA's carbohydrate recognition is unique in comparison to other antiviral lectins
4. Our results provide structural insights into the anti-HIV activity of OAA

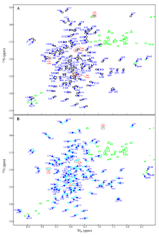

Figure 1. 2D ^{1}H-^{15}N HSQC spectra of apo (A) and α3,α6-mannopentaose-bound OAA (B)
Assignments of amide resonances (free OAA, black; α3,α6-mannopentaose-bound, cyan) are given by amino acid type and number. In both spectra, three residue pairs (S40/S107, G41/G108, and D42/D109 - labeled in red) were not unambiguously assigned since they possess degenerate Cα/Cβ chemical shifts. All side chain resonances (Trp, Arg, Asn, and Gln) are colored in green. The amide resonance of N69 was too broad for detection under the present sample conditions (25 mM NaAcetate, 25mM NaCl, 3 mM NaN_3, 90/10% H_2O/D_2O (pH 5.0), 26°C). Note that the amide resonances of G26 and G93 are significantly up-field shifted in their proton frequencies (3.38/111.7 ppm and 2.93/104.2 ppm, respectively) and not within the current spectral boundaries. See also Figures S1 and S6.

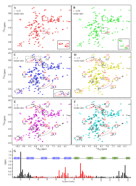

Figure 2. NMR titrations of OAA with α3, α6-mannopentaose

(A) to (F) Superposition of the 2D ^{1}H-^{15}N HSQC spectra of free (black) and α3, α6-mannopentaose bound OAA at 1:0.25 (A, red), 1:0.50 (B, green), 1:1 (C, blue), 1:1.5 (D, yellow), 1:2 (E, magenta), and at 1:3 (F, cyan) molar ratios of OAA to α3,α6-mannopentaose. Selected resonances that exhibit large chemical shift perturbations are labeled by amino acid type and number. Resonances associated with residues in binding sites 1 and 2 are colored in black and red, respectively. Insets in (A), (B), and (C) are expanded regions comprising resonances associated with binding site 2. (G) Chemical shift perturbation profile of combined amide chemical shift changes at the final titration point (1:3 molar ratio of OAA to α3,α6-mannopentaose). Values were calculated using the equation; $\Delta ppm = [(\Delta ppm\ (^{1}H_{N}))^{2} + (\Delta ppm\ (^{15}N) / 5)^{2}\ ]^{1/2}$. All spectra are plotted at the same contour level and all titrations were carried out using 0.040 mM OAA in 25 mM NaAcetate, 25mM NaCl, 3 mM NaN_3, 90/10% H_2O/D_2O (pH 5.0), 26°C. See also Figure S2.

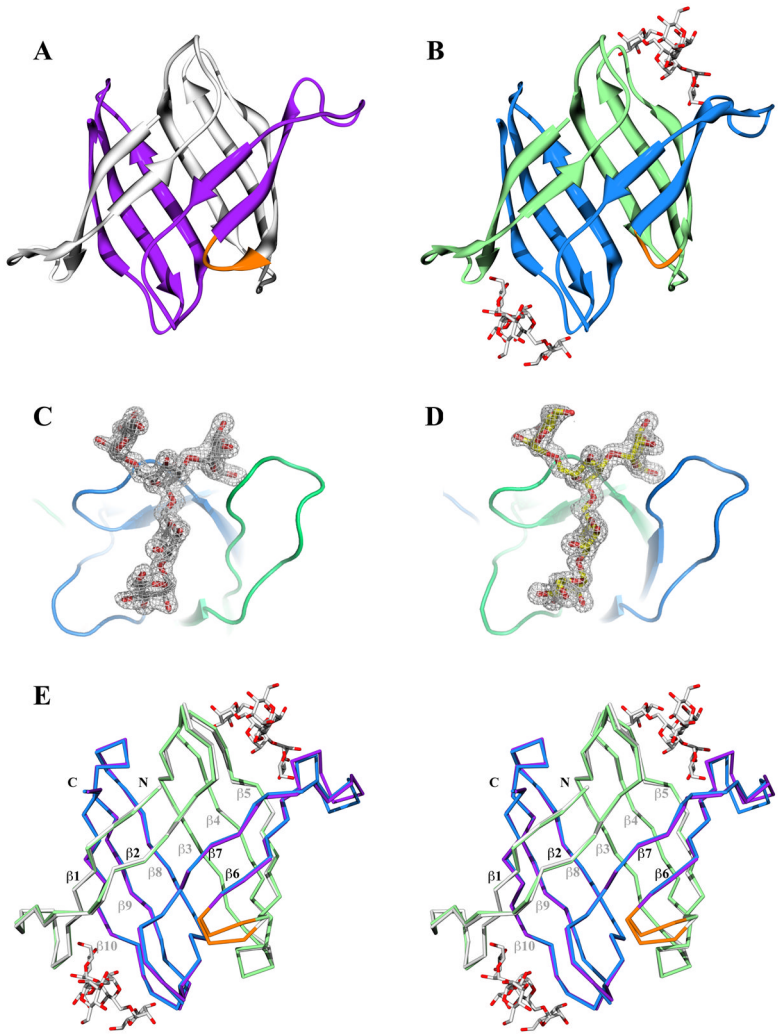

Figure 3. Crystal structures of apo and α3,α6-mannopentaose-bound OAA

(A) and (B) Ribbon representation of ligand-free and α3,α6-mannopentaose-bound OAA, respectively. The five β-strands from the first and second sequence repeats are colored white and purple in the apo structure, and light green and blue in the glycan-bound structure, respectively. The short connecting stretch between the sequence repeats (between strands β5 and β6) in both structures is colored in orange. (C) and (D) Electron density contoured at 1.0σ enclosing the molecular model of α3,α6-mannopentaose (or Manα(1-3)[Manα(1-3)[Manα(1-6)]Manα(1-6)]Man pentasaccharide) in stick representation in binding sites 1 and 2 of OAA, respectively. The surrounding protein backbone is shown in ribbon representation. (E) Stereoview of the best-fit superposition of the apo and α3,α6-mannopentaose-bound OAA structures in Cα representations. The color scheme is the same as in (A) and (B). See also Figures S3 and S7.

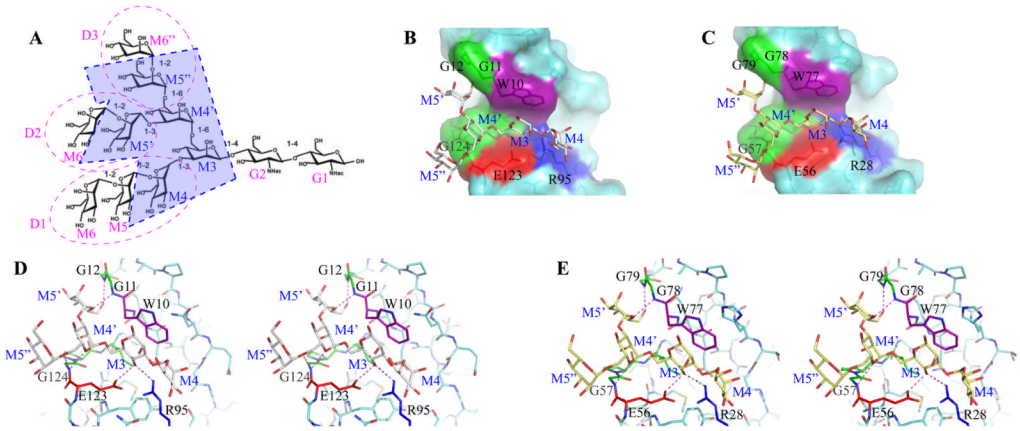

Figure 4. Details of the interaction network of α3,α6-mannopentaose in the two OAA binding sites

(A) Formula of Man-9. The α3,α6-mannopentaose, a substructure of Man-9 used in this study, is enclosed by blue dashed lines and shaded in light blue. The D1, D2 and D3 arms of Man-9 are encircled by dashed purple lines. G and M indicate N-Acetylglucosamine (GlcNAc) and Mannose (Man) units, respectively. (B) and (C) Surface representations of OAA's carbohydrate binding sites 1 and 2, respectively, with bound α3,α6-mannopentaose depicted in stick representation. Residues that are in direct contact with the carbohydrate are colored as follows; Gly, green; Trp, purple; Glu, red; and Arg, blue. The rest of the protein is in cyan. The carbohydrate molecules are shown in white and yellow for sites 1 and 2, respectively. (D) and (E) Stereoviews of bound α3,α6-mannopentaose sitting in the carbohydrate binding sites 1 and 2, respectively. Inter-molecular hydrogen bonds are indicated by magenta dashed lines. The same color scheme as in (B) and (C) is used, except that the oxygen atoms of the glycan are colored in red. Protein residues are labeled by single-letter code and the sugar rings of the carbohydrate are labeled as in (A).

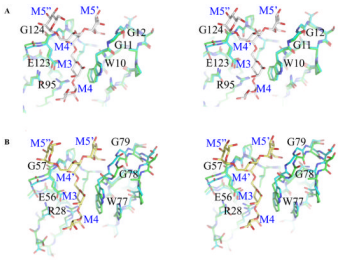

Figure 5. Structure of the carbohydrate binding pockets in apo and α3,α6-mannopentaose-bound structures

(A) and (B) Stereoviews of best-fit superpositions of OAA's carbohydrate binding sites 1 and 2, respectively, in the glycan-free (carbon atoms in green) and the α3,α6-mannopentaose-bound (carbon atoms in cyan) protein structures. The glycan molecules in binding sites 1 and 2 are shown in white and yellow, respectively, with oxygen atoms colored red. Both protein and carbohydrate in all panels are depicted in stick representations. See also Figures S3 and S7.

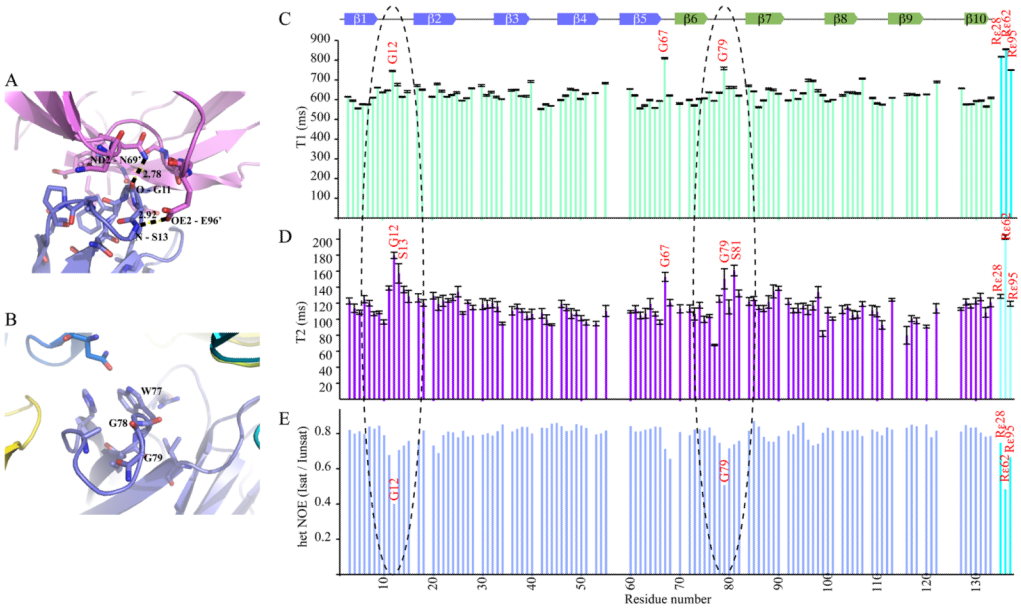

Figure 6. Crystal contacts and NMR relaxation data for apo OAA

(A) and (B) Local structure of the carbohydrate binding sites 1 (A) and 2 (B), respectively, in the apo OAA crystal structure. The conformation of the β1-β2 loop in binding site 1 is fixed in the bound conformation due to contacts with a neighboring molecule in the crystal. Inter-molecular contacts involve a hydrogen bond between the backbone carbonyl oxygen of G11 and the side chain amino group of N69’ and between the backbone amide proton of S13 and the side chain carboxyl oxygen of E96’. The equivalent loop region in binding site 2 is not in contact with any neighboring symmetrically related molecule. (C) – (E) T1, T2, and heteronuclear NOE NMR relaxation data for apo OAA. The β1-β2 and β6-β7 loops (enclosed by black dashed ovals) that line the carbohydrate binding sites 1 and 2, respectively, exhibit identical motional behavior in solution. Relaxation data for the three arginine side chains is also included at the right hand side of the graph (cyan bars). See also Figures S4 and S5.

Figure 7. Comparison of sugar-protein interactions in the α3,α6-mannopentaose bound OAA and OS-9 complexes

(A) and (B) Close-up views of the protein region sourrounding the bound carbohydrate in OAA (A) and OS-9 (B). The three mannose units of α3,α6-mannopentaose that are observed in both structures are M3 (or BMA), M4', and M5" are colored in light green (see Figure 4A for the molecular formula of Man-9). The other two mannose units of α3,α6-mannopentaose **that are** observed in OAA only are M4 and M5' (colored in light purple). Residues interacting with the glycans are colored in light blue.

Table 1

OAA data collection, phasing and refinement statistics for apo and α3,α6-mannopentaose-bound structures.

	frozen apo OAA[ac]	frozen OAA-α3,α6-mannopentaose complex[ac]	room temperature apo OAA[ac]
Data collection			
Space group	$P2_12_12_1$	$P2_12_12_1$	$P2_12_12_1$
Cell dimensions			
a, *b*, *c* (Å)	38.90 / 40.10 / 68.99	35.19 / 49.07 / 69.25	39.47 / 40.66 / 70.37
α β, γ, (°)	90 / 90 / 90	90 / 90 / 90	90 / 90 / 90
Wavelength (Å)	1.5418	1.5418	1.5418
Resolution (Å)	26.15 – 1.55 (1.61–1.55)[d]	35.19 – 1.65 (1.71–1.65)[d]	26.61 – 1.60 (1.66–1.60)[d]
R_{merge}	0.024 (0.083)[d]	0.056 (0.118)[d]	0.081 (0.309)[d]
$I / \sigma I$	52.7 (7.1)[d]	27.5 (13.2)[d]	8.7 (1.5)[d]
Completeness (%)	98.7 (89.2)[d]	96.4 (87.4)[d]	95.0 (91.5)[d]
Redundancy	6.00 (2.99)[d]	12.02 (8.91)[d]	2.48 (1.80)[d]
Refinement			
Resolution (Å)	34.67 1.55 (1.59–1.55)[d]	40.04 1.65 (1.69–1.65)[d]	35.20 1.60 (1.64–1.60)[d]
No. unique reflections	15,223	13,024	13,272
R_{work} / R_{free}	0.181 / 0.193 (0.242 / 0.299)[d]	0.178 / 0.219 (0.231 / 0.308)[d]	0.182 / 0.228 (0.247 / 0.302)[d]
No. atoms			
Protein	993	1004	1004
Ligand/ion	1	112	-
Water	149	127	62
B-factors			
Protein	10.39	17.33	27.07
Ligand/ion	33.83	20.23	-
Water	19.60	26.17	36.89
R.m.s deviations			
Bond lengths (Å)	0.011	0.012	0.022
Bond angles (°)	1.282	1.532	1.933

[a]Data were obtained from the best diffracting crystal according to crystallization condition (see text for details).

[b] Crystallographic phases were obtained by molecular replacement using the previously determined structure of OAA in triclinic *P1* space group (PDB:3OBL).

[c] Refinement was carried out using Refmac5.

[d] Values in parentheses are for highest-resolution shell.